

## Physicochemical stability under inert and reductive atmospheres of $\text{Li}_2\text{TiO}_3$ produced from $\text{Li}_2\text{CO}_3$ obtained from Argentinean brines

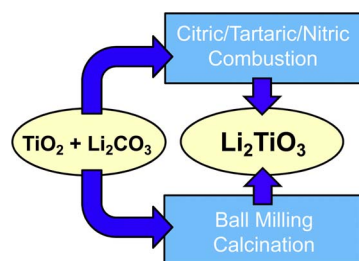
I.A. Carbajal-Ramos<sup>a,c</sup>, J.L. Zacur<sup>b</sup>, J. Andrade-Gamboa<sup>a,\*</sup>, N. Palacios<sup>b</sup>, M. Rodriguez<sup>b</sup>, F.C. Gennari<sup>a,c</sup>

<sup>a</sup> Centro Atómico Bariloche, Av. Bustillo 9500, Bariloche, Río Negro, Argentina

<sup>b</sup> Facultad de Ingeniería, Universidad Nacional de Jujuy, Ítalo Palanca 10, Jujuy, Argentina

<sup>c</sup> Consejo Nacional de Investigaciones Científicas y Técnicas (CONICET), Argentina

### GRAPHICAL ABSTRACT



### ARTICLE INFO

#### Keywords:

Tritium breeder  
 $\text{Li}_2\text{TiO}_3$   
 Microstructure  
 Hydrogen  
 Thermal stability

### ABSTRACT

Lithium metatitanate ( $\text{Li}_2\text{TiO}_3$ ) is one of the most promising candidates as tritium breeder material in a fusion reactor due to its physical and chemical properties. In this paper, the syntheses of  $\text{Li}_2\text{TiO}_3$  by combustion in solution (SCS) and solid-solid (SSS) were developed using as raw material  $\text{Li}_2\text{CO}_3$  produced from Argentinean brines and  $\text{TiO}_2$ . In SCS, aqueous solution of  $\text{Li}_2\text{CO}_3$  and  $\text{TiO}_2$  as metal precursors, citric/tartaric acids as complexing agent/fuel and  $\text{HNO}_3$  as oxidant was formed, heated to dryness and then self-combusted. The solid obtained was calcined at  $550^\circ\text{C}$  for 12 h to obtain nanometric  $\text{Li}_2\text{TiO}_3$  (monoclinic phase, 90%), with particle sizes  $< 0.5\ \mu\text{m}$  and meso/macropores. In SSS,  $\text{Li}_2\text{CO}_3\text{-TiO}_2$  mixture was ball milled in air at room temperature and subsequently annealed. The effect of milling time and calcined temperature in the formation of  $\text{Li}_2\text{TiO}_3$  was studied. High yields of  $\text{Li}_2\text{TiO}_3$  ( $> 90\%$  and  $99\%$ ) were obtained even at low heating temperatures ( $400$  and  $600^\circ\text{C}$  for 24 h, respectively). The synthesized powders show mean grain sizes in the nanometric range, particle sizes  $< 0.7\ \mu\text{m}$  and macropores. Changes that occur during heat treatment in inert and slightly reductive atmospheres ( $5\% \text{H}_2/\text{Ar}$ ) were identified.

The SSS and SCS methods developed using easy to handle and low-priced precursors constitute cost-attractive processes for large scale production of  $\text{Li}_2\text{TiO}_3$  nanopowders.

### 1. Introduction

The breeding blanket is a key component of fusion reactors because it directly involves the tritium breeding and energy extraction, both

critical aspects to the development of fusion energy processes. In current designs, the solid breeding blanket is formed by the breeder (lithium compound), a coolant for heat removal and a structural material containing and supporting the breeder [1]. The breeder is responsible to

\* Corresponding author at: Centro Atómico Bariloche, Av. Bustillo, km 9500, San Carlos de Bariloche (8400), Río Negro, Argentina.  
 E-mail address: [andrade@cab.cnea.gov.ar](mailto:andrade@cab.cnea.gov.ar) (J. Andrade-Gamboa).

<https://doi.org/10.1016/j.fusengdes.2018.03.022>

Received 31 August 2017; Received in revised form 19 February 2018; Accepted 8 March 2018  
 0920-3796/ © 2018 Published by Elsevier B.V.

produce tritium by reaction with neutrons and release it to maintain the fuel cycle within the reactor, according to the following reaction:



Lithium ceramic such as  $\text{Li}_2\text{TiO}_3$ ,  $\text{Li}_4\text{SiO}_4$ ,  $\text{Li}_2\text{ZrO}_3$  are considered potential candidates [1,2]. In particular, monoclinic lithium metatitanate ( $\beta\text{-Li}_2\text{TiO}_3$ ) is one of the most promising as tritium breeding materials in the D-T fusion reactors owing to its high lithium atom density, good compatibility with structural materials and its good tritium release property. Several physicochemical properties are demanded on these materials and they are depending of the microstructure and final composition achieved during the synthesis procedure [2,3]. Considering that a fusion power plant of 1 GW could require approximately 30 Tn per year of  $\text{Li}_2\text{TiO}_3$  containing natural lithium [4], it is evident the importance to develop synthesis procedure for industrial purposes.

Numerous methods have been developed to produce  $\text{Li}_2\text{TiO}_3$  powders such as solid-state (thermal treatment, mechanical milling, urea assisted solid state) [5–10] and wet-chemistry methods (sol-gel [11,12], combustion [13–16], hydrothermal [17–19], in-situ hydrolysis method [20]). Further performance of the ceramic in operating conditions (reductive atmosphere, high temperature, irradiation effects) is strongly dependent of the synthesis procedure, the presence of impurities and the final microstructure obtained. Among the possible methods, the solution combustion synthesis (SCS) is an effective procedure for the production of nanoscale materials and offer well-known advantages of liquid phase reactions with respect to solid phase reactions [21–23]. The metal precursors in an aqueous solution are mixed with the fuel (glycine, urea, sucrose) and oxidizers (nitrates, sulfates). The dispersion of reactants takes place optimally producing a homogeneous mixture and increasing the reactivity of precursors. After preheating to the ignition temperature, the reaction begins and provides the heat for reaction sustainability, producing valuable products. SCS has the advantage of rapidly producing fine and homogeneous powders. In addition, it is a simple and efficient method for the scalable synthesis of mixed oxide powders, saving time and energy.

One major drawback in some wet-chemistry methods is the high volume of liquid or gaseous waste generated. As alternative, solid-state synthesis (SSS) emerges as potential option for the preparation of stoichiometric single-phase material but this procedure usually requires high-temperature of thermal treatment to favor the diffusion of the components.

To overcome this drawback, the use of high energy mechanical milling in combination with post annealing allows the production of amorphous and/or nanocrystalline metal/non-metal composite materials at lower temperatures [24–26]. In the ball milling step, plastic deformation, cold-welding and fracture are predominant factors, which leads to the refinement of the microstructure (particle and grain sizes reduction) and surface/bulk defects generation [24]. These modifications improve the posterior reactivity of the components and the final product could be obtained at lower temperature in comparison with the traditional solid-state reaction.

In this work,  $\text{Li}_2\text{TiO}_3$  powders were prepared by two different synthesis procedures: combustion reaction in solution (SCS) and solid-solid synthesis (SSS). These procedures were designed to use as raw material,  $\text{Li}_2\text{CO}_3$  obtained from Argentinean brines and commercial  $\text{TiO}_2$ . According to the literature [10–17,19], the usual lithium precursors for the wet chemical synthesis of  $\text{Li}_2\text{TiO}_3$  are lithium hydroxide and lithium nitrate. High purity  $\text{Li}_2\text{CO}_3$  is available in the North of Argentina. It is obtained by vaporization, precipitation and refinement of natural brines containing lithium in addition to other ions and is the main source in the manufacture of lithium battery electrodes, an increasingly important device in the accumulation and transport of energy. The stability, availability and low comparative price of this local precursor makes it attractive for the syntheses proposed in this paper, seeking to expand the possible applications of the resource in the

generation of energy through DT fusion reactors. On the other hand, the use of cheaper and easy to handle  $\text{TiO}_2$  in comparison with other conventional titanium sources ( $\text{TiCl}_4$  [11],  $\text{TiO}(\text{NO}_3)_2$  [13,15], Tetra-butyltitanate [10,16]) provides an economical benefit.

Microstructural, chemical, structural and textural characteristics of the powders produced by SCS and SSS were studied. In addition, thermal behavior of the  $\text{Li}_2\text{TiO}_3$  in both He and  $\text{H}_2(5\%)/\text{He}$  flows were evaluated to identify possible mass loss mechanisms. This work was developed as part of the activities in the subprogram of controlled nuclear fusion at CNEA (National Commission of Atomic Energy, Argentina).

## 2. Experimental

The starting material were  $\text{Li}_2\text{CO}_3$  (98%) produced in Argentina from natural brines and  $\text{TiO}_2$  (Aldrich, 99%) powders. Other chemical reagents were of analytical purity and were used without additional purification.

For SCS an aqueous solution was prepared using stoichiometric  $\text{Li}_2\text{CO}_3$  and  $\text{TiO}_2$  as lithium and titanium precursors, respectively. The chelating-fuel and oxidant agents selected were citric/tartaric acids and  $\text{HNO}_3$ . The molar ratio citric acid, tartaric acid to total nitrate was 1.8:1:0.3. The mixed solution was heated at  $70^\circ\text{C}$  with continuously stirring for several hours till the solution became yellowish sol. After that, the sol changed into a dry-gel and it was auto-ignited by a self-propagating combustion yielding a solid product. This material was milled in a mortar and heated at  $550^\circ\text{C}$  for 12 h to produce a white powder.

For SSS, the  $\text{Li}_2\text{CO}_3\text{-TiO}_2$  mixture (1:1 mol ratio) was milled under air at room temperature for different times (10 min, 0.5 h, 1 h, 5 h) using a planetary ball mill (Fritsch Pulverisette P6). The milling chamber and the balls were of stainless steel. The experimental milling conditions were ball to powder weight ratio of 53:1 and operation at 400 rpm. The as-milled powders were annealed at  $400^\circ\text{C}$ ,  $600^\circ\text{C}$  and  $800^\circ\text{C}$  for different times. The yield of the synthesis procedure was determined by calculation of the ratio between the mass of desired product ( $\text{Li}_2\text{TiO}_3$ ) and the total mass.

Crystal structure of the powders was studied by X-ray Powder Diffraction (XRPD, PANalytical Empyrean, con  $\text{CuK}\alpha$  and graphite monochromator). The estimations of mean grain size (D) and microstrains ( $\epsilon$ ) were performed by Williamson-Hall method ( $\Gamma_{\text{instrumental}} = 0.065^\circ$ ) [27]. Microstructure was observed by Scanning Electron Microscopy (SEM Nova Nano 230, FEI Company) equipped with EDS (Energy Dispersive Spectroscopy) for chemical microanalysis. Textural characteristics of the powders were studied using a Micromeritics ASAP 2020 analyzer.  $\text{N}_2$  adsorption isotherms were collected at  $-196^\circ\text{C}$  on 0.2 g of sample, after evacuation at  $350^\circ\text{C}$  overnight. Surface area and pore distribution were obtained applying the BET and BJH methods, respectively.

Physicochemical stability of the samples as a function of the temperature and the atmosphere was evaluated using thermogravimetry (TG, TA Instruments HP50) and temperature programmed reduction (TPR, Micromeritics AutoChem 2910). For TPR runs, the mixture 5%  $\text{H}_2/\text{Ar}$  ( $100 \text{ cm}^3/\text{min}$ ) was introduced into the reactor containing 0.25 g of sample and 30 min were waited up to flow stabilization. Then, the temperature was increased from room temperature up to  $800^\circ\text{C}$  using  $10^\circ\text{C}/\text{min}$  ramp. Hydrogen consumption was monitored using TCD detector. When  $\text{CO}_2$  is generated due to  $\text{Li}_2\text{CO}_3$  decomposition, an internal calibration was performed to quantify  $\text{CO}_2$ . For TG measurements,  $\sim 0.12 \text{ g}$  were heated under gas flow (He or  $\text{H}_2(5\%)/\text{Ar}$ ). The sample, previously heated at  $200^\circ\text{C}$  for 1 h under dry inert gas, was heated from room temperature to  $800^\circ\text{C}$  using a  $10^\circ\text{C}/\text{min}$  ramp and  $50 \text{ cm}^3/\text{min}$  flow. Solid phase IR spectra were obtained with an FTIR Perkin Elmer Spectrum 400 spectrometer in the range of  $800\text{--}4000 \text{ cm}^{-1}$ . The selected samples were grounded with dry KBr, pressed to pellets and put in specially designed cell in air.

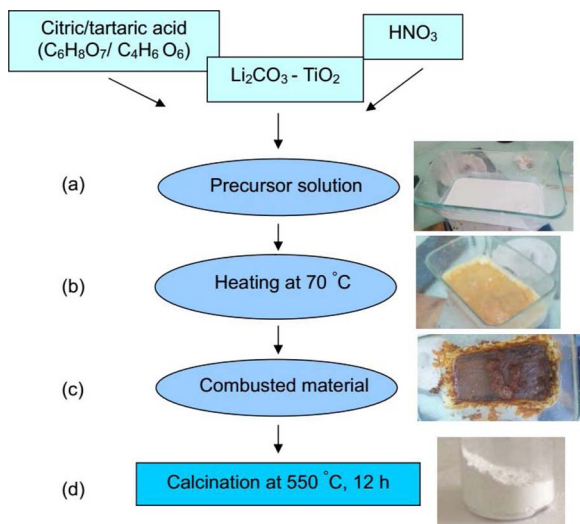
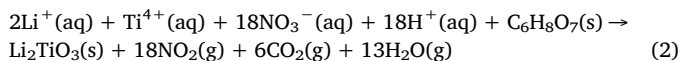


Fig. 1. Scheme of the solution combustion synthesis route to produce  $\text{Li}_2\text{TiO}_3$ .

### 3. Results and discussion

#### 3.1. Synthesis of $\text{Li}_2\text{TiO}_3$ by different synthesis procedures

A scheme of the SCS route and the representative photographs of materials at different stage of the  $\text{Li}_2\text{TiO}_3$  synthesis are shown in Fig. 1. Lithium and titanium precursors and  $\text{HNO}_3$  were stirred to obtain a white dispersion (Fig. 1a). Tartaric and citric acids were added and then the solution was heated up to  $80^\circ\text{C}$  on a hot plate under continuous stirring until all liquid evaporated. The starting mixture changes from white to yellow color (Fig. 1b). There was evolution of fumes towards the end of the reaction leaving a fluffy mass in the recipient. The reaction is completed by self-combustion giving a brown product (Fig. 1c). At this point, the powder was milled and calcined at  $550^\circ\text{C}$  for 12 h to obtain a white powder (Fig. 1d). The global reaction of the SCS route can be represented as:



After annealing, the final phases were analyzed by XRPD (Fig. S1) and the composition of mixture was monoclinic- $\text{Li}_2\text{TiO}_3$  (90 wt%),  $\text{TiO}_2$  as rutile (2 wt%) and  $\text{Li}_2\text{CO}_3$  (8 wt%). The yield of the synthesis procedure was 90%.

The SSS route is depicted in Fig. 2. The XRPD patterns obtained after 10 min, 1 h and 5 h of milling show the presence of both starting materials. No evidence of reaction induced by mechanical processing was detected between  $\text{Li}_2\text{CO}_3$  and  $\text{TiO}_2$  from XRPD patterns. As an example, Fig. 3 displays the X-ray diffractogram of the  $\text{Li}_2\text{CO}_3$ - $\text{TiO}_2$  mixture after 1 h of milling. It can be seen the most intense peaks of the

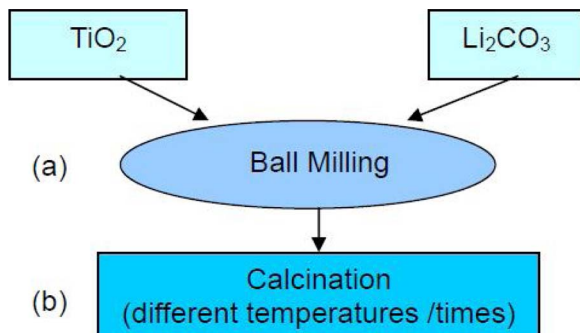


Fig. 2. Scheme of the solid-state synthesis route to produce  $\text{Li}_2\text{TiO}_3$ .

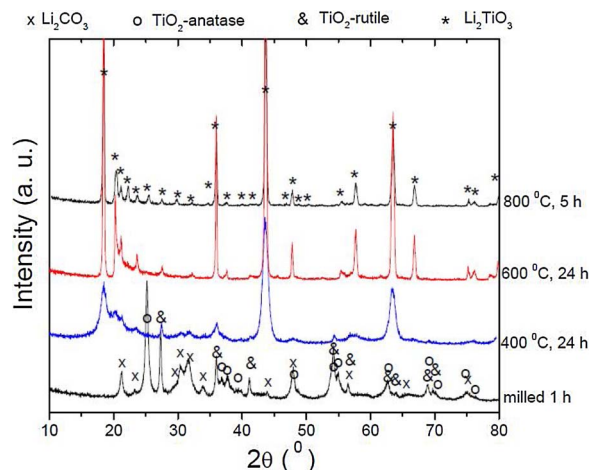
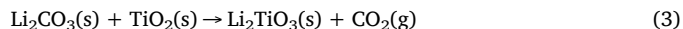


Fig. 3. XRPD patterns of the  $\text{Li}_2\text{CO}_3$ - $\text{TiO}_2$  mixture after 1 h of milling, annealed at  $400^\circ\text{C}$  (24 h),  $600^\circ\text{C}$  (24 h) and  $800^\circ\text{C}$  (5 h).

$\text{Li}_2\text{CO}_3$  and  $\text{TiO}_2$  (anatase and rutile phases). Then, the mechanical milling favors the physical mixture between the reactants without promotion of the reaction between them. On the other hand, it is known that mechanical milling induces microstructural modifications in the starting materials, such as reduction in the grain size and or introduction of microstrains, which could favor further reaction between reactants with temperature raising [24,26].

The  $\text{Li}_2\text{CO}_3$ - $\text{TiO}_2$  mixture after 1 h of milling was annealed at different temperatures and times. Fig. 3 shows the evolution of the  $\text{Li}_2\text{TiO}_3$  formation with the temperature. After heating at  $400^\circ\text{C}$  for 24 h the most intense diffraction peaks of  $\text{Li}_2\text{TiO}_3$  are identified as well as those corresponding with  $\text{Li}_2\text{CO}_3$  and  $\text{TiO}_2$  (rutile). Similar thermal treatment at  $600^\circ\text{C}$  (24 h) and  $800^\circ\text{C}$  (5 h) leads to the complete formation of  $\text{Li}_2\text{TiO}_3$ , without evidence of remnant starting materials. The solid state reaction can be expressed as:



The brittle nature of the starting materials avoid the adherence between the powders and the milling chamber, which possibilities their posterior recovery for the thermal treatment. The SSS procedure has a yield  $> 99\%$ .

To clarify the influence of the milling time on the  $\text{Li}_2\text{TiO}_3$  formation during thermal treatment, samples milled for different times were annealed at  $600^\circ\text{C}$  for 24 h. The XRPD patterns are shown in Fig. 4. For

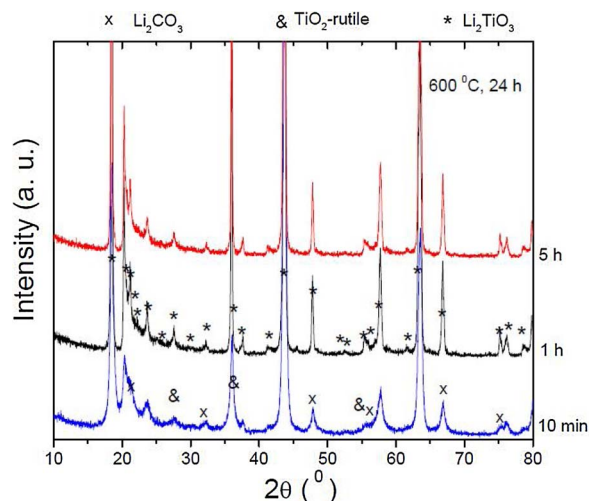


Fig. 4. XRPD patterns of the  $\text{Li}_2\text{CO}_3$ - $\text{TiO}_2$  mixture milled 10 min, 1 h and 5 h and afterwards annealed at  $600^\circ\text{C}$  (24 h).

mixture milled for 10 min and annealed, besides  $\text{Li}_2\text{TiO}_3$  presence also the starting materials are identified, which indicates the incomplete  $\text{Li}_2\text{TiO}_3$  formation. On the contrary, the combination of 1 h of milling (or 5 h) and equal thermal treatment (24 h,  $600^\circ\text{C}$ ) induces the complete formation of  $\text{Li}_2\text{TiO}_3$  and the complete  $\text{Li}_2\text{CO}_3$  consumption. By comparison of the results shown in Figs. 3 and 4, for a thermal treatment of  $600^\circ\text{C}$  during 24 h, milling for 1 h is enough to produce the desired material. For the next studies it was selected  $\text{Li}_2\text{TiO}_3$  produced under moderate conditions because the short milling time (1 h) minimizes possible contamination with the material of the milling chamber and balls, and the intermediate temperature ( $600^\circ\text{C}$ ) of annealing reduces the energetic consumption.

Therefore, SCS and SSS allow the production of  $\text{Li}_2\text{TiO}_3$  with high yield, using as starting materials precursors of low cost and good chemical stability:  $\text{Li}_2\text{CO}_3$  obtained from Argentinean natural resources and  $\text{TiO}_2$ . These synthesis procedures constitute valuable production methods on the industrial scale. In the case of SSS, the combination of mechanical milling and thermal treatment reduces the  $\text{Li}_2\text{TiO}_3$  formation temperature and the overall energetic requirements in comparison with the conventional ceramic synthesis. Production of  $\text{Li}_2\text{TiO}_3$  by SCS requires low temperature, short time and simple equipment, resulting in an energy-efficient method.

### 3.2. Characterization of $\text{Li}_2\text{TiO}_3$ powders produced by SCS and SSS routes

Samples of  $\text{Li}_2\text{TiO}_3$  produced by SCS and SSS were studied to characterize their morphology, microstructure, structure, chemical composition and texture. Fig. 5 show the micrographs of SEM for both samples (magnifications  $50000\times$  and  $100000\times$ ). The powder obtained

by SSS displays a compact and homogeneous morphology, with particle sizes lower than  $0.7\ \mu\text{m}$  (Fig. 5A) which are linked and/or sintered (Fig. 5C). Due to the neck grain growth, the shape of the particles is not clear but the presence of pores is even visible. In opposition, the powders produced by SCS show an open microstructure, with pores clearly identified between the particles (Fig. 5B). The existence of connected pores is expected to provide large internal surface for tritium and helium release during irradiation [28,29]. The particles have rounded and defined edges with a wide distribution of sizes from  $0.1\ \mu\text{m}$  to  $0.5\ \mu\text{m}$  (Fig. 5D). For the samples produced by SCS and SSS routes, several EDS analyses were performed on wide areas ( $200\ \mu\text{m} \times 200\ \mu\text{m}$ ) to identify possible contaminations. Minor amounts of Si (Si/Ti ratio lower than 2 at.%) were detected in the sample produced by SCS method. No Fe contamination was noticed in the  $\text{Li}_2\text{TiO}_3$  powders produced by SSS.

From XRPD patterns of Figs. S1 and Figure 4, it can be estimated the cell parameters of the samples produced by SCS and SSS which are, within the experimental error, similar than the reported values (ICDD-PDF card #33-831). The mean grain size calculated for the  $\text{Li}_2\text{TiO}_3$  powders produced by SCS method is about 70 nm (microstrain,  $\epsilon = 0.6\%$ ). For the sample milled 1 h and annealed at  $600^\circ\text{C}$  for 24 h the mean grain size is 130 nm ( $\epsilon = 0.1\%$ ). This information indicates that each particle identified by SEM is an agglomeration of single-crystal domains.

Textural characterization of the  $\text{Li}_2\text{TiO}_3$  powders obtained by both methods was performed by nitrogen physisorption (Fig. 6). The isotherm for  $\text{Li}_2\text{TiO}_3$  produced by SCS is Type II (according IUPAC classification) and presents a slight hysteresis, which indicates the presence of macropores ( $> 50\ \text{nm}$ ) and some mesopores. The specific surface

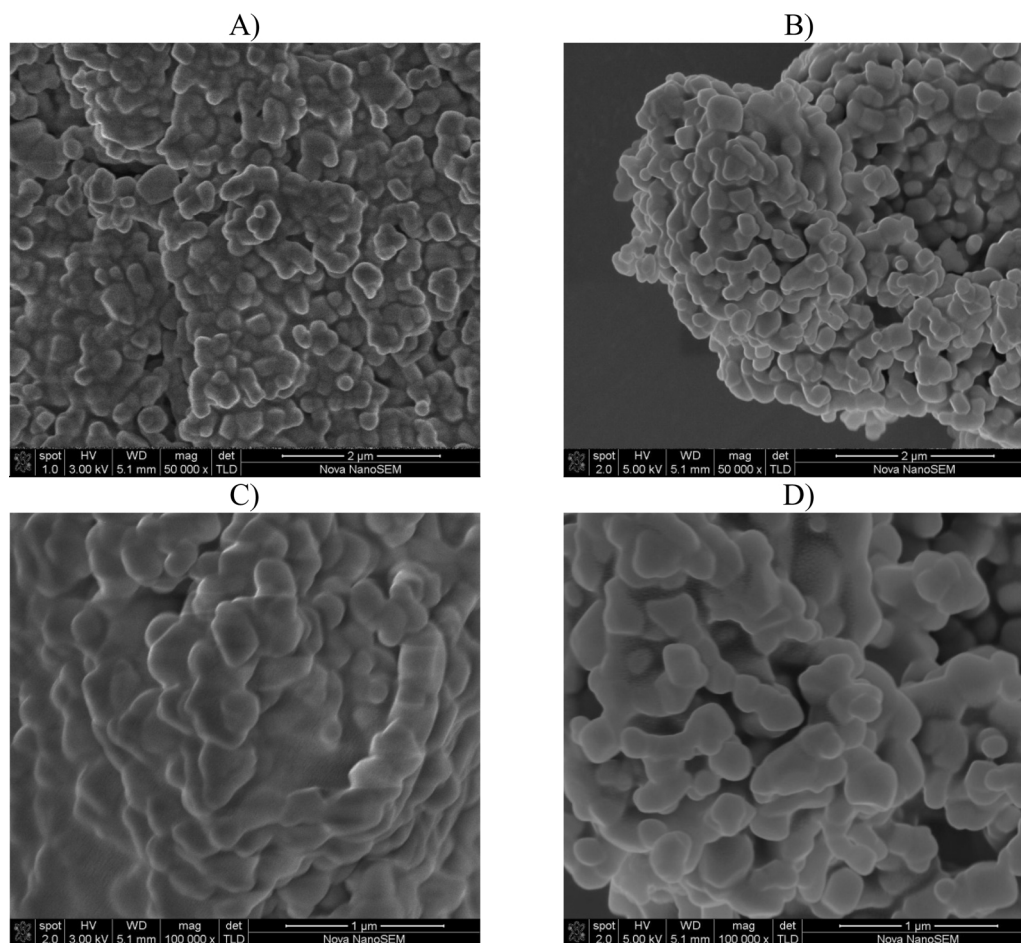


Fig. 5. SEM micrographs of the powders obtained by SSS (A, C) and SCS (B, D).

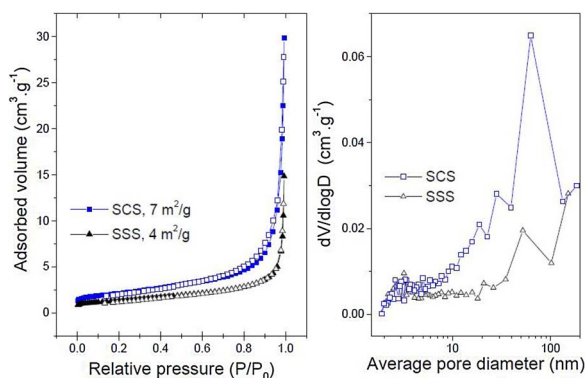


Fig. 6. Adsorption/desorption isotherm of nitrogen for as-synthesized  $\text{Li}_2\text{TiO}_3$  powders produced by SCS and SSS.

area is  $7 \text{ m}^2/\text{g}$ . In the case of SSS, it was observed an isotherm type II, without hysteresis, with a surface specific area of  $4 \text{ m}^2/\text{g}$  and macropores presence. Then, the material obtained by SCS has higher area than those produced by SSS, with a porous microstructure (meso and macropores), smaller grain size and particles with smaller size (associated with several crystallographic domains). The small grain size obtained for  $\text{Li}_2\text{TiO}_3$  using both synthesis procedure is promising, considering that the final grain size affect the tritium release ability and thermal conductivity, being optimum values less than  $5 \mu\text{m}$  [30].

It is important to remark that in SCS the microstructure of the products can be controlled by fuel type, fuel-to-oxidizer ratio and combustion mode [23]. In particular, citric acid can act as a fuel and also as complexant for metal ions avoiding precipitation. A recent work studied the effect of the fuel-to-oxidizer ratio on both the combustion mode and the microstructure of the  $\text{Li}_2\text{TiO}_3$  powders [16]. A crystallite size of  $\text{Li}_2\text{TiO}_3$  between 18 and 36 nm and density more than 90% of theoretical density (TD) were obtained by sintering at low temperature ( $800^\circ\text{C}$ ), which avoids grain size increasing and sintering. These results evidence the potentiality of SCS as an effective method for the production of nanoscale  $\text{Li}_2\text{TiO}_3$ , with controlled microstructure and sinterability by an adequate control of the synthesis parameters.

### 3.3. Physicochemical stability of the $\text{Li}_2\text{TiO}_3$ powders produced by SCS and SSS routes under different atmospheres

It is known that lithium ceramics such as  $\text{Li}_2\text{TiO}_3$  absorb moisture and carbon dioxide from the air to produce  $\text{LiOH}(\text{H}_2\text{O})$  and/or  $\text{Li}_2\text{CO}_3$  compounds. Thermal treatments of these ceramics under dry conditions induces both  $\text{LiOH}(\text{H}_2\text{O})$  and  $\text{Li}_2\text{CO}_3$  decomposition into  $\text{Li}_2\text{O}$  and gaseous species such as  $\text{H}_2\text{O}$  and  $\text{CO}_2$  [31]. On the other hand, in the blanket of DT fusion reactors it is expected that the tritium generated by the lithium ceramics has to be swept by He gas or  $\text{H}_2(100 \text{ Pa})/\text{He}$  mixed gas to obtain a high tritium recovery efficiency, assuming that physorbed species were removed before operation [32]. In fact, the tritium produced by the breeder could interact physically and/or chemically with the breeding material itself, both with species in the surface and/or with the bulk. Hence, it is important to investigate the aging behavior of  $\text{Li}_2\text{TiO}_3$  in inert and reductive flows existing during sweep gas conditions. To analyze the physicochemical stability of the material during the thermal treatment under inert atmosphere (He), the mass loss of the  $\text{Li}_2\text{TiO}_3$  powders as a function of temperature was measured using a heating ramp of  $10^\circ\text{C}/\text{min}$  (Fig. 7). The as-synthesized  $\text{Li}_2\text{TiO}_3$  powders show different behavior, depending of the synthesis procedure. The SSS sample has a small mass loss (about 1–1.5%, curve a). Considering that the sample was handled under atmospheric conditions, the mass loss can be related from FTIR measurements with the presence of moisture (broad band at  $3420 \text{ cm}^{-1}$ ) and carbonate species ( $1430$  and  $1506 \text{ cm}^{-1}$ ) onto the powders surface (see Fig. S2-A). The band at  $1635 \text{ cm}^{-1}$  is related with  $\text{H}_2\text{O}$  vibration of atmospheric water

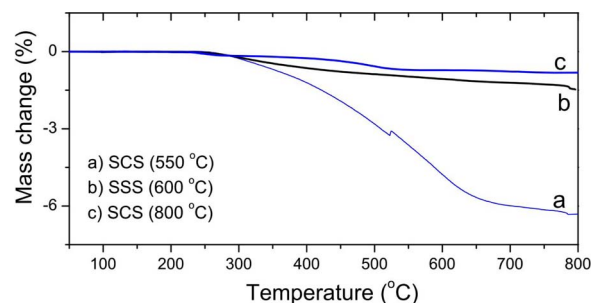


Fig. 7. TG curves under helium flow for SSS and SCS samples: a) as-synthesized SCS; b) as-synthesized SSS; c) SCS calcined at  $800^\circ\text{C}$  for 5 h.

vapor. In the case of SCS sample, the presence of un-reacted  $\text{Li}_2\text{CO}_3$  (8 wt%, determined by XRPD) is the responsible of about 4.5% of the mass loss measured due to  $\text{CO}_2$  releasing (Fig. 7, curve b). In addition, an extra mass loss of about 1.5% is possible by similar species than in the case of SSS sample (see Fig. S2-A), i.e. moisture and  $\text{CO}_3^{2-}$  anions due to the surface absorption of  $\text{CO}_2$  [33]. As important point, no bands corresponding to organic residual compounds were detected in the FTIR spectrum of SCS sample.

To corroborate these interpretations, the SCS sample was ex-situ annealed in air at  $800^\circ\text{C}$  (Fig. 7, curve c) to complete  $\text{Li}_2\text{CO}_3$  decomposition. FTIR performed on this sample after short atmospheric exposition confirms the elimination of moisture and a reduction of surface carbonates species (Fig. S2-B). After this, the mass change of this sample was evaluated as a function of temperature in He flow. The mass loss observed in He for SCS sample treated at  $800^\circ\text{C}$  was the smallest ( $< 1\%$ ). At the end of the TG measurements, the samples were analyzed by XRPD. The only phase detected was monoclinic  $\text{Li}_2\text{TiO}_3$  and no evidence of the presence of other species was found.

To evaluate the behavior of the samples under reductive atmosphere, programmed temperature reduction measurements were performed using  $\text{H}_2(5\%)/\text{Ar}$  flow up to  $800^\circ\text{C}$ . The TCD signal as a function of temperature is shown in Fig. 8. The as-synthesized SCS and SSS samples show different behavior, with a peak centered at  $680$  and  $650^\circ\text{C}$ , respectively, being the signal three times higher for the SCS sample. The SSS sample consumed a low amount of hydrogen ( $83 \mu\text{mol g}^{-1}$ ), which was detected due to the high sensibility of the TCD detector. In the case of SCS sample, the presence of unreacted  $\text{Li}_2\text{CO}_3$  (confirmed in TG measurement, Fig. 7a) leads to the superposition of the signals of  $\text{CO}_2$  release and hydrogen consumption. Using an internal calibration for  $\text{CO}_2$  and assuming 8 wt% of  $\text{Li}_2\text{CO}_3$ , the amount of hydrogen consumed in the SCS sample was  $62 \mu\text{mol g}^{-1}$ . Then, both samples display the same order of magnitude of the

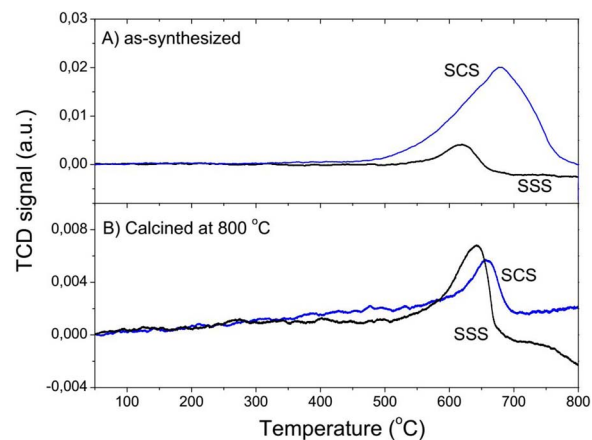


Fig. 8. TPR curves of SCS and SSS samples. A) as-synthesized; B) calcined at  $800^\circ\text{C}$ . Heating ramp:  $10^\circ\text{C}/\text{min}$ ,  $\text{H}_2(5\%)/\text{Ar}$ , flow:  $100 \text{ cm}^3/\text{min}$ .

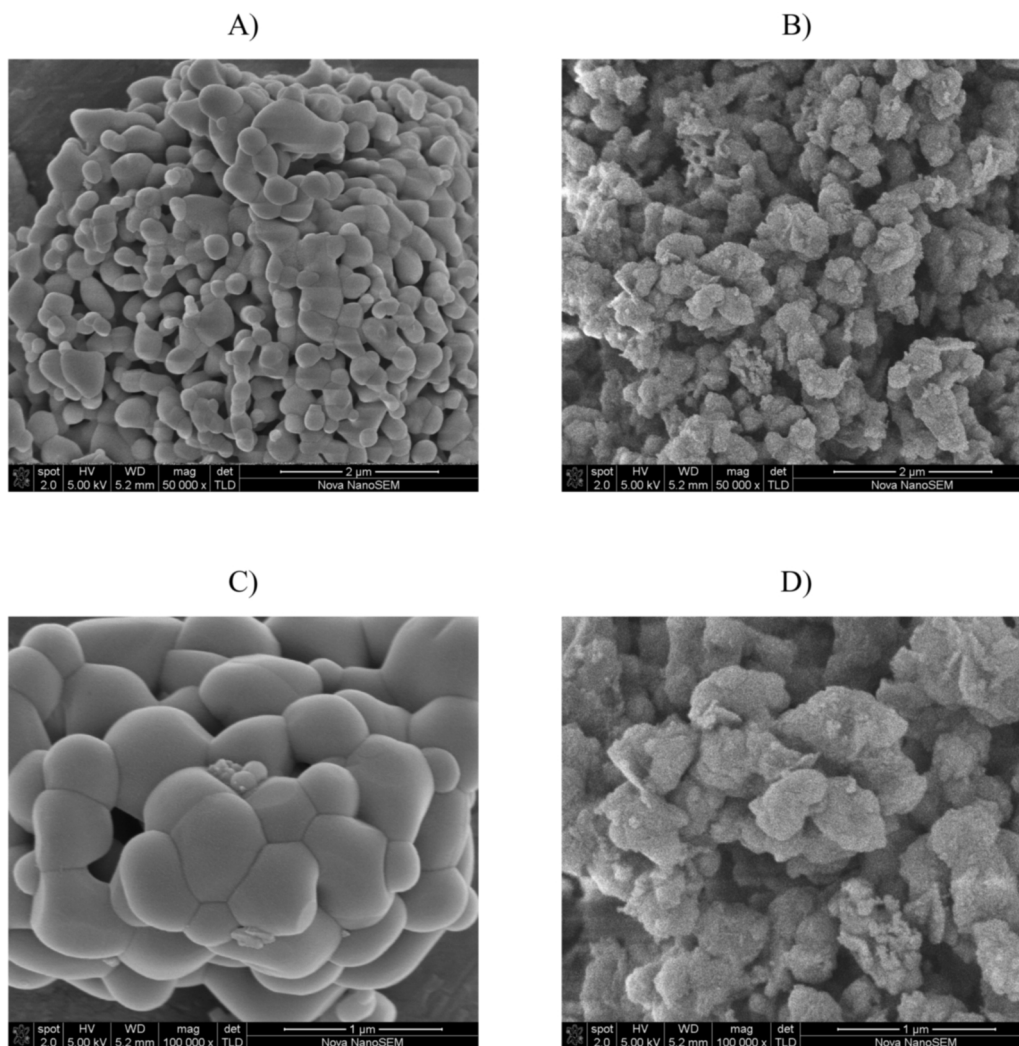
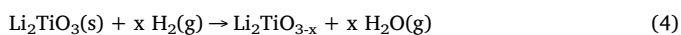


Fig. 9. SEM micrographs of the powders obtained by SSS (A, C) and SCS (B, D) after reduction under  $H_2(5\%)/Ar$  flow.

reduction, according the reaction



with  $x$  values is between 0.0068 and 0.0091.

Extra TPR curves of SCS and SSS samples after calcination at  $800^\circ C$  show similar shape and amount of hydrogen consumed (between 60 and  $90 \mu mol g^{-1}$ ). In addition, for SSS sample, the TPR curve after calcination at  $800^\circ C$  is similar than that obtained as-synthesized. The powders show a change in the color from white to blue, which could be associated with some defects formation due to reduction. The white color could be recovered by heating of the powder under air.

The microstructure of the as-synthesized samples after the reduction was studied using SEM. The photographs are shown in Fig. 9(A–D) (magnification  $50000\times$  y  $100000\times$ ). It can be seen that SSS sample has particles with size ( $0.5\text{--}0.7 \mu m$ ) similar those observed before reduction (Fig. 5). Some elimination of porosity and the formation of defined grain structure were observed due to a minor degree of sintering. As a difference, the SCS sample shows disaggregated particles, with edge and shape undefined probably due to the  $CO_2$  releasing.

XRPD patterns obtained with the samples at the end of the TPR curves reveal the presence of  $Li_2TiO_3$ , without evidence of other detectable changes in the structure. These results suggest that  $Li_2TiO_3$  powders are relatively stable under hydrogen flow and only a small reduction is detected, even when the hydrogen content ( $5\%H_2/He$ ) is higher than that used in the sweep gas. All results constitute evidence of the comparatively high thermal stability of  $Li_2TiO_3$  obtained by SSS

method.

Finally, SSS and SCS methods allow the production of  $Li_2TiO_3$  powders with particle sizes lower than  $0.7 \mu m$  and minimum grain growth, even after thermal treatment at  $800^\circ C$  under inert or reductive atmospheres. Special attention is devoted to SCS method due to the possibility to modify different parameters that influence the microstructure. The  $Li_2TiO_3$  powders produced using citric acid/fuel ratio 6:1 show the presence of interconnected pores and crystallite sizes lower than those obtained by SSS, all factors considered beneficial for the tritium and helium release during irradiation [28–30]. Although a 90% of TD required for fusion application [34,35] could be obtained from  $Li_2TiO_3$  powders produced by SCS [16], it is known that lithium density decreases during operation conditions due to burn-up. For this reason, advanced breeder materials such as a mixture of  $Li_2TiO_3$  ( $0.44 g/cm^3$ ) with  $Li_4SiO_4$  ( $0.54 g/cm^3$ ) [36,37] among others [35] are being studied to improve the lithium density in  $Li_2TiO_3$ . Consequently, it is necessary to advance in the development of improved breeder materials as well as in their experimental evaluation under irradiation conditions.

#### 4. Conclusions

Powders of  $Li_2TiO_3$  were successfully synthesized, using same starting materials, by combustion solution technique and ball milling followed by thermal treatment. Both  $Li_2CO_3$  and  $TiO_2$  were selected as precursors due to their availability, simple handling and low cost in comparison with the usual lithium and titanium precursors selected in

wet chemical methods. SCS allows producing monoclinic  $\text{Li}_2\text{TiO}_3$ , with crystallite size of 70 nm, a specific area of  $7\text{ m}^2/\text{g}$ , macropores ( $> 50\text{ nm}$ ) and some mesopores. SSS exhibits higher yield, given nanopowders of mean grain size of 130 nm, specific area of  $4\text{ m}^2/\text{g}$  and macropores.

The as-synthesized  $\text{Li}_2\text{TiO}_3$  powders by SCS and SSS show the presence of moisture and carbonate species on the surface after handling under atmospheric conditions. These species were eliminated by heating at  $800\text{ }^\circ\text{C}$  under He flow. This thermal treatment improves sample stability for posterior exposition to air. Independently of the synthesis procedure, the samples display a limited reducibility under  $\text{H}_2(5\%)/\text{He}$ , even if the material was annealed at  $600\text{ }^\circ\text{C}$  (24 h) or  $800\text{ }^\circ\text{C}$  (5 h).

The microstructure of the synthesized materials and their thermal stability after surface cleaning both in inert and reduced atmospheres is promising as breeder material for DT fusion reactors. The synthesis methods developed can be scaled-up and cost-effective for the industrial production of  $\text{Li}_2\text{TiO}_3$ .

### Acknowledgements

This study has been partially supported by CNEA (National Commission of Atomic Energy), ANPCyT and CONICET (National Council of Scientific and Technological Research). The authors thank to the Microscopy National Service provided by the Gerencia de Investigación Aplicada – Department of Materials Characterization (CAB-CNEA) and Dr. Facundo Castro for the TG measurements.

### Appendix A. Supplementary data

Supplementary data associated with this article can be found, in the online version, at <https://doi.org/10.1016/j.fusengdes.2018.03.022>.

### References

- [1] R.J.M. Konings, *Comprehensive Nuclear Materials*, Elsevier, Spain, 2012.
- [2] R. Knitter, P. Chaudhuri, Y.J. Feng, T. Hoshino, I.-K. Yu, Recent developments of solid breeder fabrication, *J. Nucl. Mater.* 442 (Suppl. 1) (2013) S420–S424.
- [3] E. Carella, M. Gonzalez, R. Gonzalez-Arrabal, D-depth profiling in as-implanted and annealed Li-based breeder blanket ceramics, *J. Nucl. Mater.* 438 (2013) 193–198.
- [4] J. Wesson, *Tokamaks*, 3rd ed., Oxford University Press, 2004.
- [5] Z.-F. Fu, P. Liu, J.-Li Ma, Fabrication nanopowders by high-energy ball-milling and low temperature sintering  $\text{Li}_2\text{TiO}_3$  microwave dielectrics, *Mater. Sci. Eng. B* 193 (2015) 32–36.
- [6] D. Mandal, D. Sathiyamoorthy, V. Govardhana Rao, Preparation and characterization of lithium-titanate pebbles by solid-state reaction extrusion and spheroidization techniques for fusion reactor, *Fusion Eng. Des.* 87 (2012) 7–12.
- [7] I.A. Carbajal-Ramos, J.J. Andrade-Gamboa, A.M. Condó, F.C. Gennari, Formation of cubic  $\text{Li}_2\text{TiO}_3$  by mechanical activation and its transformation to monoclinic phase: stability in helium and hydrogen flows, *Solid State Ionics* 308 (2017) 46–53.
- [8] Y.-H. Park, K.-M. Min, S. Cho, M.-Y. Ahn, Y.-M. Lee,  $\text{Li}_2\text{TiO}_3$  powder synthesis by solid-state reaction and pebble fabrication for tritium breeding material, *Fusion Eng. Des.* 124 (2017) 730–734.
- [9] B.M. Tripathi, T. Mohanty, D. Prakash, A.K. Tyagi, P.K. Sinha, Monoclinic  $\beta\text{-Li}_2\text{TiO}_3$  nanocrystalline particles employing novel urea assisted solid state route: synthesis, characterization and sintering behavior, *J. Nucl. Mater.* 490 (2017) 167–173.
- [10] M. Hong, Y. Zhang, Y. Mi, Y. Jiang, M. Xiang, Synthesis of  $\text{Li}_2\text{TiO}_3$  by sol-gel combustion method and its gel-casting formation, *J. Nucl. Mater.* 455 (2014) 311–315.
- [11] T.V. Vittal Rao, Y.R. Bamankar, S.K. Mukerjee, S.K. Aggarwal, Preparation and characterization of  $\text{Li}_2\text{TiO}_3$  pebbles by internal gelation sol-gel process, *J. Nucl. Mater.* 426 (2012) 102–108.
- [12] T. Hoshino, F. Oikawa, Trial fabrication tests of advanced tritium breeder pebbles using sol-gel method, *Fusion Eng. Des.* 86 (2011) 2172–2175.
- [13] Q. Zhou, L. Tao, Y. Gao, L. Xue, Y. Yan, Flash synthesis of  $\text{Li}_2\text{TiO}_3$  powder by microwave-induced solution combustion, *J. Nucl. Mater.* 455 (2014) 101–105.
- [14] A. Sinha, S.R. Nair, P.K. Sinha, Single step synthesis of  $\text{Li}_2\text{TiO}_3$  powder, *J. Nucl. Mater.* 399 (2010) 162–166.
- [15] I.C.H. Jung, J.Y. Park, S.J. Oh, H.K. Park, Y.S. Kim, D.K. Kim, J.H. Kim, Synthesis of  $\text{Li}_2\text{TiO}_3$  ceramic breeder powders by the combustion process, *J. Nucl. Mater.* 253 (1998) 203–212.
- [16] Q. Zhou, Y. Mou, X. Ma, L. Xue, Y. Yan, Effect of fuel-to-oxidizer ratios on combustion mode and microstructure of  $\text{Li}_2\text{TiO}_3$  nanoscale powders, *J. Eur. Ceram. Soc.* 34 (2014) 801–807.
- [17] W. Zhang, Q. Zhou, L. Xue, Y. Yan, Fabrication of  $\text{Li}_2\text{TiO}_3$  pebbles with small grain size via hydrothermal and improved dry-rolling methods, *J. Nucl. Mater.* 464 (2015) 389–393.
- [18] A. Laumann, K. Thomas Fehr, M. Wachsmann, M. Holzapfel, B. Brummerstedt Iversen, Metastable formation of low temperature cubic  $\text{Li}_2\text{TiO}_3$  under hydrothermal conditions — its stability and structural properties, *Solid State Ionics* 181 (2010) 1525–1529.
- [19] I.K. Mukai, K. Sasaki, T. Terai, A. Susuki, T. Hoshino, Observations on microstructure and crystal structure of sintered lithium metatitanate with excess Li, *Fusion Eng. Des.* 87 (2012) 836–839.
- [20] Y.J. Li, C. Xu, X. Wang, L. Li, L. Kong, Synthesis of  $\text{Li}_2\text{TiO}_3$  ceramic breeder powders by in-situ hydrolysis and its characterization, *Mater. Lett.* 89 (2012) 25–27.
- [21] A. Kopp Alves, C.P. Bergmann, F.A. Berutti, *Novel Synthesis and Characterization of Nanostructured Materials*. Chap. 2: Combustion Synthesis, Springer-Verlag, Berlin Heidelberg, 2013.
- [22] S.T. Aruna, A.S. Mukasyan, Combustion synthesis and nanomaterials, *Curr. Opin. Solid State Mater. Sci.* 12 (2008) 44–50.
- [23] A.S. Rogachev, A.S. Mukasyan, *Combustion for Materials Synthesis*, CRC Press Taylor & Francis Group, Boca Raton, 2015.
- [24] C. Suryanarayana, *Mechanical Alloying and Milling*, Marcel Dekker, New York, 2004.
- [25] D. Domanski, G. Urretavizcaya, F. Castro, F.C. Gennari, Mechanochemical synthesis of magnesium aluminum spinel powder at room temperature, *J. Am. Ceram. Soc.* 87 (11) (2004) 2020–2024.
- [26] I.A. Carbajal-Ramos, J.J. Andrade-Gamboa, F.C. Gennari, Nanostructured  $\text{Ce}_{1-x}\text{Zr}_x\text{O}_2$  solid solutions produced by mechanochemical processing, *Mater. Chem. Phys.* 137 (2013) 1073–1080.
- [27] G.K. Williamson, W.H. Hall, X-ray line broadening from filed aluminium and wolfram, *Acta Metall.* 1 (1953) 22–31.
- [28] S. Sharafat, N. Ghoniem, M. Sawan, A. Ying, B. Williams, Breeder foam: an innovative low porosity solid breeder material, *Fusion Eng. Des.* 81 (2006) 455–460.
- [29] T. Tanifuji, D. Yamaki, T. Takahashi, A. Iwamoto, Tritium release from neutron-irradiated  $\text{Li}_2\text{O}$  sintered pellets: porosity dependence, *J. Nucl. Mater.* 283–287 (2000) 1419–1423.
- [30] T. Kinjyo, M. Nishikawa, M. Enoeda, S. Fukada, Tritium diffusivity in crystal grain of  $\text{Li}_2\text{TiO}_3$  and tritium release behavior under several purge gas conditions, *Fusion Eng. Des.* 83 (2008) 580–587.
- [31] M. Hara, Y. Togashi, M. Matsuyama, Y. Oya, K. Okuno, Crystal structure change of  $\text{Li}_{2+x}\text{TiO}_{3+y}$  tritium breeder under moist air, *J. Nucl. Mater.* 404 (2010) 217–221.
- [32] T. Hanada, M. Nishikawa, T. Kanazawa, H. Yamasaki, N. Yamashita, S. Fukada, Effect of surface water on tritium release behavior from  $\text{Li}_2\text{TiO}_3$ , *J. Nucl. Mater.* 417 (2011) 735–738.
- [33] Y. Furuyama, Y. Sasaki, Y. Gotoh, A. Taniike, A. Kitamura, Composition change of the near-surface layer of  $\text{Li}_2\text{TiO}_3$  after  $\text{CO}_2$  absorption observed with accelerator analyses, *J. Nucl. Mater.* 442 (2013) S442–S446.
- [34] J.G. van der Laan, A.V. Federov, S. van Til, J. Reimman, Ceramic breeder materials, in: R. Konings (Ed.), *Comprehensive Nuclear Materials*, 1st ed., Elsevier Science, 2012, pp. 463–510.
- [35] S. Konishi, M. Enoeda, M. Nakamichi, T. Hoshino, A. Ying, S. Sharafat, S. Smolentsev, Functional materials for breeding blankets—status and developments, *Nucl. Fusion* 57 (2017) 092014 (19 pp).
- [36] D.A.H. Hanaor, M.H.H. Kolb, Y. Gan, M. Kamlah, R. Knitter, Solution based synthesis of mixed-phase materials in the  $\text{Li}_2\text{TiO}_3\text{-Li}_4\text{SiO}_4$  system, *J. Nucl. Mater.* 456 (2015) 151–161.
- [37] M.H.H. Kolb, K. Mukai, R. Knitter, T. Hoshino,  $\text{Li}_4\text{SiO}_4$  based breeder ceramics with  $\text{Li}_2\text{TiO}_3$ ,  $\text{LiAlO}_2$  and  $\text{Li}_x\text{La}_y\text{TiO}_3$  additions, part I: fabrication, *Fusion Eng. Des.* 115 (2017) 39–48.